# Long-range microscopic PTV of inner layer turbulence over a superhydrophobic surface with random texture

**Wagih Abu Rowin**
Department of Mechanical Engineering
University of Alberta
Canada, Edmonton AB T6G 2G8
aburowin@ualberta.ca

**Jianfeng Hou**
Department of Mechanical Engineering
University of Alberta
Canada, Edmonton AB T6G 2G8
hou6@ualberta.ca

**Sina Ghaemi***
Department of Mechanical Engineering
University of Alberta
Canada, Edmonton AB T6G 2G8
ghaemi@ualberta.ca

## ABSTRACT

Microscopic particle tracking velocimetry (micro-PTV) and macroscopic particle image velocimetry (PIV) are simultaneously carried out to characterize the turbulent structure of both the inner and outer layers over a superhydrophobic surface (SHS). The SHS is produced by spray coating with small roughness of $k^+_{rms}$ = 0.11 (root-mean-square of wall roughness normalized by wall unit). The channel flow is operated at $Re_H$ = 4,400 (based on full channel height and 0.174 m/s average velocity). The micro-PTV measurement shows 0.023 m/s slip velocity over the SHS (about 13% of the bulk velocity), which corresponds to a slip-length of about 200 μm. The reduction of skin friction is about 22% based on the analytical expression of Rastegari & Akhavan (2015). The peak of the streamwise Reynolds stress over SHS is shifted toward the wall by $\Delta y^+$ ~ 5 relative to the smooth wall. The wall-normal Reynolds stress over SHS is smaller than the smooth surface at $y^+$ >10. Reynolds shear stress over the SHS at $y^+$>10 is smaller than Reynolds shear stresses over the smooth surface. The longevity of the SHS is also investigated by characterizing temporal evolution of near-wall velocity using micro-PTV.

## INTRODUCTION

A thin layer of air at the interface between liquid flow and a solid surface can form a shear-free interface and potentially reduce skin-friction drag. A method of introducing the air layer is using superhydrophobic surfaces (SHSs), which typically have a nano- or micro-scale surface texture or pattern. The texture can be obtained by various methods, for example, by spray coating of chemically hydrophobic particles (Rothstein, 2010). The phenomenon when an air layer is trapped between the SHS and the liquid is called the Cassie state, as shown in Figure 1(a). However, in the Wenzel state, the air layer is depleted and there will be a direct contact between the surface and the fluid as shown in Figure 1(b) (Papadopoulos et al. 2013).

The magnitude of the slip velocity over a SHS and consequently the reduction in skin-friction is expected to depend on the surface area and topography of the air pockets. This hypothesis has been confirmed in the laminar regime where a 40% skin-friction reduction (SFR) based on pressure drop was observed in a micro-channel by Ou et al. (2004). The application of SHSs to the turbulent regime has been evaluated by several experiments showing possibility of large SFR (e.g., 50% SFR by Daniello et al., 2009; 75% SFR by Park et al., 2013).

The investigation of the velocity field over SHSs in turbulent wall flows has been mostly carried out in the outer layer using macroscopic PIV. Zhang et al. (2015) observed a considerable increase of mean velocity up to $y/\delta \approx 0.5$ over a SHS ($\delta$ is boundary layer thickness). However, Woolford et al. (2009) and Vajdi Hokmabad & Ghaemi (2016) observed a negligible change in the mean velocity profile in the outer layer of a turbulent channel flow, suggesting the variation of the mean velocity is limited to the inner layer. These two investigations also observed a 5-10% reduction of Reynolds stresses over the SHS.

To the authors' knowledge, only Ling et al. (2016) investigated the inner layer of a turbulent boundary layer over random patterned SHSs using digital holographic microscopy. Their observation showed a maximum SFR of 36% over a SHS based on a 46% reduction of viscous shear stress and a 10% increase of Reynold shear stress at the wall. The latter is associated with the relatively large roughness of $k^+_{rms}$ = 0.68 (root-mean-square of wall roughness normalized by wall unit) of their SHS.

The current investigation evaluates the variation of slip velocity and Reynolds shear stress over a SHS with smaller roughness ($k^+_{rms}$ = 0.11) relative to Ling et al. (2016). Macroscopic PIV and long rang micro-PTV are carried out in a fully developed turbulent channel flow to characterize the mean velocity profile and Reynolds stresses in both the inner and outer layers. The measurements are carried out

simultaneously to ensure the inner and outer layer measurements are over a common plastron morphology.

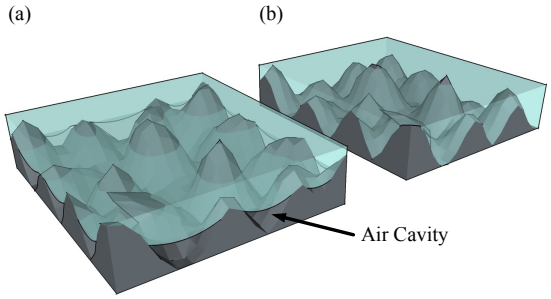


Figure 1. A schematic of a random texture SHS in (a) Cassie state, and (b) Wenzel state.

## EXPERIMENTAL SETUP

### Flow Facility

The experiments are carried out in a turbulent channel flow embedded inside a flume. The channel is formed by a glass bottom wall, a cast acrylic top wall, side walls, and a honeycomb structure at the entrance as shown in Figure 2. The channel is 3 m long in the streamwise direction ($x$) with a rectangular cross-section of 25 mm ($H$) in the wall-normal direction ($y$) and 540 mm in the spanwise direction ($z$) as shown in Figure 2. The top plate has an insert located 1.9 m (76$H$) downstream of the entrance, which is 550 mm long and 300 mm wide. The flume is seeded with 5 μm hollow glass spheres with a density of 1.016 g/cm$^3$.

The average velocity across the channel is $U_b$ = 0.174 m/s. The flow rate is kept constant in the flume using an orifice flow meter with an estimated time-averaged variation of ±0.002 m/s in $U_b$ based on repeating the experiments. The Reynolds number based on full channel height ($H$) is $Re_H$ = 4,400. The estimated wall unit is $\lambda$ = 88.8 μm and the friction velocity is $u_\tau$ = 0.0113 m/s based on micro-PTV over the smooth acrylic wall. The friction Reynolds number is $Re_\tau$ = 140. In the present experiment, the thickness of the viscous sublayer is estimated to be 444 μm. The channel dimensions and flow condition are summarized in Table 1. The superscript $^+$ represents parameters normalized using friction velocity $u_\tau$ and wall unit $\lambda$ of the smooth surface.

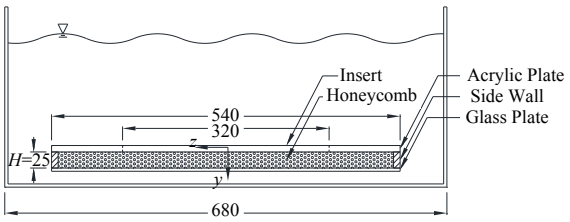


Figure 2. The cross section of the channel embedded inside the larger flume. The inner channel has a honeycomb at the entrance.

### Superhydrophobic Surfaces

A random pattern SHS is produced by spray coating. The insert plate was first cleaned with ethanol followed by two steps of superhydrophobic coating (Rust-Oleum NeverWet) in a fume hood. The first step is the base layer for better adhesion of the superhydrophobic particles. Three layers of top coating were applied to deposit the mico/nano particles. The surface was allowed to dry for 12 hours. The coating roughness is $k^+_{rms}$ = 0.11 (root-mean-square of wall roughness normalized by wall unit) based on measurements of Vajdi Hokmabad & Ghaemi (2016). Bidkar et al. (2014) has shown that SFR is observed when the surface roughness of a SHS is an order of magnitude smaller than the thickness of viscous sublayer. As shown in the flow facility section, the thickness of viscous sublayer is estimated 444 μm which is an order of magnitude larger than the SHS peak-to-trough roughness of $k_{pt}$ =40 μm (Vajdi Hokmabad & Ghaemi 2016).

Table 1. The geometric dimensions and flow statistics of the turbulent channel flow.

| Parameter | Value |
|---|---|
| Channel dimensions ($H$×$W$×$L$) (mm) | 25×540×3,000 |
| $U_b$ (m/s) | 0.174 |
| $U_{max}$ (m/s) | 0.205 |
| $Re_H$ | 4,400 |
| $u_\tau$ (m/s) | 0.0113 |
| $\lambda$ (μm) | 88.8 |
| $Re_\tau$ | 140 |

### Particle image velocimetry

Planar PIV measurements are carried out over a field-of-view (FOV) of 45.5 mm × 28.5 mm at digital resolution of 32.6 μm/pix using an Imager Intense CCD camera (sensor size of 1040×1376 pix, pixel size of 6.45×6.45 μm$^2$, and 12-bit resolution). The FOV is located 94$H$ downstream of the channel entrance and 15$H$ downstream of the leading-edge of the insert plate. The illumination is provided by a 400 mJ/pulse Nd:YAG laser (Spectra-Physics). A collimated laser sheet of 1 mm thickness is formed using spherical and cylindrical lenses and directed parallel to the channel wall by a mirror sealed in an acrylic column downstream of the channel to minimize wall reflection. An ensemble of 8,000 pairs of double-frame images ($\Delta t$ = 1500 μs) are recorded at 5 Hz for each case.

The image processing (Davis 8.3 /LaVision Gmbh) initiates with subtraction of the minimum of the ensemble of the PIV images from each individual image. The images are also normalization by the average intensity of the ensemble to increase the signal-to-noise ratio before applying the cross-correlation algorithm. Multi-pass ensemble of correlations (EOC) with initial interrogation window (IW) size of 96×96 and final IW size of 8×8 pixels (0.2×0.2 mm$^2$, 2.9$^+$×2.9$^+$) with 75 percent overlap is applied. The location of the top and bottom walls for PIV measurements are detected by plotting the intensity profile of the images along $y$ direction averaged over the ensemble of the images and also along $x$ direction. The intensity peak ($I_{max}$) formed due to the remaining small reflection of the laser sheet represents the wall location. The upper bound uncertainty of this technique is equivalent to the thickness of the glare

line, which is estimated using the width of the intensity peak at $I_{max}/e^2$. This is equivalent to 5 pix (163.5 μm, $1.8^+$).

### Long-range microscopic particle tracking velocimetry

PTV with high-spatial resolution is carried out using a second Imager Intense CCD camera (LaVision GmbH) equipped with a Nikkor lens with focal length of $f$ = 200 mm at aperture size of $f$ /11. The lens is connected to 360 mm extension tube (bellows) to allow a working distance of 370 mm. The combination results in magnification of $M$ = 1.6 and digital resolution of 3.92 μm/pix. The estimated depth-of-field of 0.3 mm is smaller than the laser sheet thickness (~1 mm), therefore, presence of out-of-focus particle images is expected. PTV measurements are carried out 85$H$ downstream of the channel entrance and 9$H$ downstream of the leading-edge of the insert plate. The FOV is 5.3 mm×4.0 mm in the $x$ and $y$ directions, respectively. An ensemble of 8,000 pairs of double-frame images were recorded for micro-PTV with $\Delta t$ = 1500 μs, allowing maximum displacement of 70 pix in streamwise direction. Minimum intensity subtraction and image normalization was applied before carrying out particle tracking. The number density of the particles in the images is around 4 particles per mm$^2$. Wall detection has been carried out similar to the method applied to the PIV images. The estimated uncertainty based on the PTV images is 1.5pix = 5.8μm = $0.06^+$.

The PTV algorithm was developed in MATLAB to only track the in-focus particles. The algorithm initiates by detection of local maxima which are larger than the threshold intensity. The local maxima are rejected if multiple peaks are detected within a rectangular window of 60×45 pix in $x$ and $y$ directions, respectively. This filter prevents detection of erroneous pairs in the subsequent steps. The area of particle images is estimated and particles outside of 3-10 pixels are rejected. Particle images smaller than 3 pix in area can introduce bias error due to peak locking (Kähler et al. 2012) while particles larger than 10 pix are speculated to be out-of-focus. The pair detection is carried out using an initial predictor obtained by EOC of the PTV images (Meinhart et al. 2000). A multi-pass EOC with initial window size of 256×256 pixel to detect the large particle movements is followed by smaller window size of 8×8 (31.3×31.3 mm$^2$) with 75 percent overlap. The PTV algorithm applied the estimated velocity from EOC to search for the particle in the second frame in a ($\Delta x$, $\Delta y$) = 60×30 pix neighborhood of the estimated location. The out-of-focus particles do not have a distinguished peak and their pattern is different in the two frames. Therefore, only particle pairs with peak intensity ratio of 0.25 – 1.8 are selected for the final sub-pixel peak detection using a Gaussian filter with kernel of 12×12 pixels.

The average velocity and high-order turbulence statistics are obtained by averaging the particle velocities sorted in bins based on their wall-normal location. The mean velocity profile is obtained by averaging over ($\Delta x$, $\Delta y$) = 1290×10 pix (5.0×0.04 mm$^2$, $56.9^+$×$0.44^+$) bins while the second-order statistics (Reynolds stresses) are obtained by averaging over larger bins with ($\Delta x$, $\Delta y$) = 1290×100 pix (5.0×0.39 mm$^2$, $56.9^+$×$4.4^+$) to ensure statistical convergence.

## RESULTS AND DISCUSSION

The turbulent flow is characterized over smooth (baseline) and SHS. The SHS is located at $y$ / $H$ = 0 while the glass surface is located at $y$ / $H$ = 1 in both smooth and SHS cases. DNS data at $Re_\tau$ = 150 by Tsukahara et al. (2005) is used as a reference in all Reynolds stresses plots. The longevity of the SHS is also investigated by scrutiny of the temporal variation of average velocity in time.

### Mean Velocity

The semi-logarithmic presentation of normalized mean streamwise velocity ($u^+ = \langle U \rangle / u_\tau$) over the smooth surface obtained from micro-PTV and PIV (using EOC method) is shown in Figure 3. The PTV profile shows a perfect overlap with both the law of the wall ($u^+ = y^+$) in the linear sublayer and the logarithmic law ($u^+ = 1/\kappa \ln(y^+) + B$) profile with $\kappa$ = 0.39 and $B$ = 5.5. The overlap indicates a fully developed turbulent channel flow. There is a small discrepancy between the PIV data and PTV data at $y^+$<20 which is associated with bias errors and limited spatial resolution in the near wall PIV measurement (Theunissen et al. 2008).

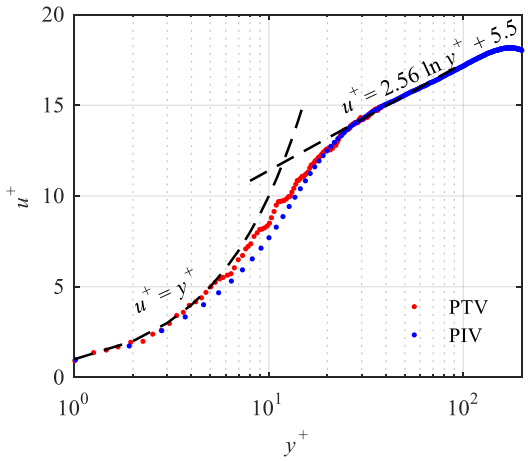


Figure 3. Mean velocity profiles over the smooth wall obtained from the micro-PTV and PIV (using EOC).

Scrutiny of the near-wall velocity is carried out using the long-range micro-PTV. The velocity distribution of individual PTV tracers over the smooth surface and SHS in the inner layer ($y^+$<35) is shown in Figure 4 and 5, respectively. Mean velocity obtained from averaging the particle velocities in bins with ($\Delta x$, $\Delta y$) = $56.9^+$×$0.44^+$ dimensions are also shown in these figures. The presence of the no-slip boundary condition is evident over the smooth surface as the mean velocity approaches zero at the wall ($y^+$ = 0) and the detected tracers also have a negligible velocity in the immediate vicinity of the wall. There is a large number of particles with finite velocity $1 \le U^+ \le 4$ (0.011 m/s $\le U \le$ 0.044 m/s) at the immediate vicinity of the SHS. The estimated mean slip velocity is $U_s$ = 0.023 m/s ($U^+$ = 2.1) at $y^+$= 0 over the SHS which is about 13% of the bulk velocity. Ling et al. (2016) reported slip velocities in the

order of 14.5 to 36.5% of $U_b$ (0.29 to 0.73 m/s, or $3.2^+$ to $9.6^+$) on different SHSs with $k^+_{rms}$ ranging from 0.43 and 3.28. In the laminar flow, Ou & Rothstein (2005) observed slip velocity up to 60% of $U_b$ with 20 μm slip-length over ultra-hydrophobic surface in microchannel with $Re < 1000$.

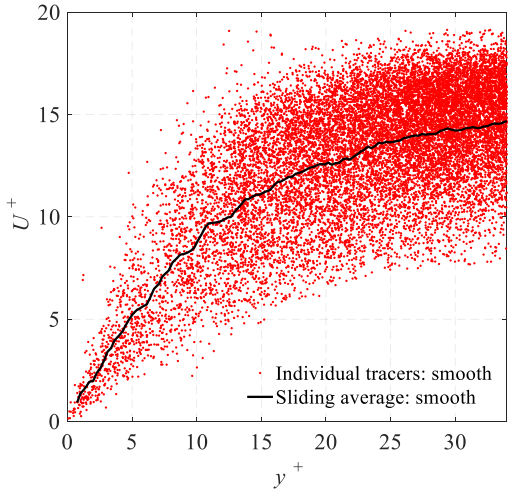


Figure 4. The velocity of tracer particles from micro-PTV over smooth surface.

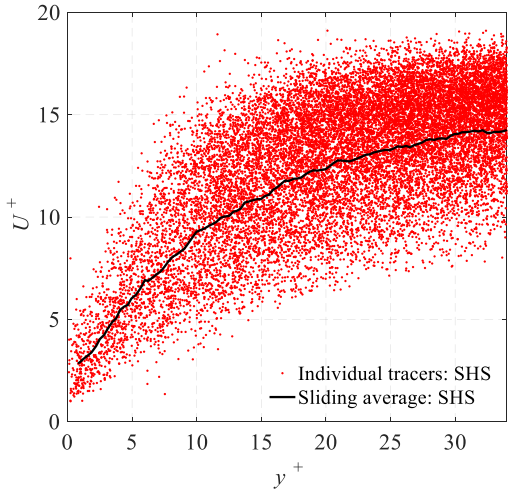


Figure 5. The velocity of tracer particles from micro-PTV over the SHS.

## Reynolds shear stress

The near-wall $\langle uv \rangle$ over the smooth and SHS obtained by micro-PTV is shown in Figure 6. The wall-normal distance is normalized by the inner scaling ($\lambda$). Reynolds shear stress over the SHS is slightly larger than the smooth surface at $y^+<10$ while it becomes significantly smaller ($\sim 0.1 u_\tau^2$) further away from the wall at $y^+ = 35$. The experiments of Woolford et al. (2009) showed overlap of $\langle uv \rangle$ profiles on the half of the channel where the common flat surface is located, while $\langle uv \rangle$ slope of the SHS becomes gradually smaller than the smooth one with approaching the SHS wall. They observed about 10% reduction of $\langle uv \rangle$ peak intensity with no displacement of the its location over a SHS with streamwise grooves, producing 11% reduction of wall shear stress. Measurements of Ling et al. (2016) over a SHS with high DR with roughness $k^+ \geq 0.89$ showed a larger $\langle uv \rangle$ over the SHSs at $y^+<15$ followed by smaller $\langle uv \rangle$ at $15<y^+<100$. However, this trend was different over the larger roughness $k^+ \geq 1.71$ since they observed larger $\langle uv \rangle$ over all the investigated region of $2<y^+<100$.

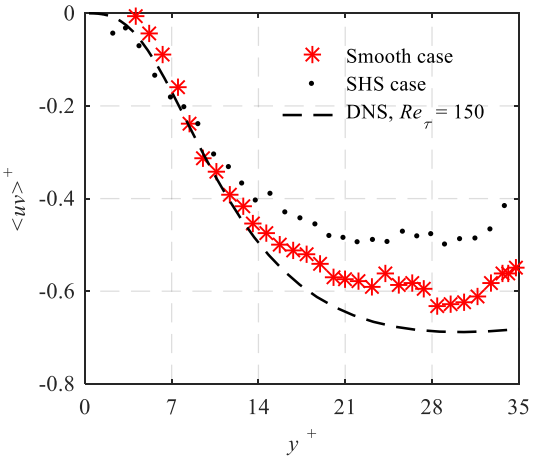


Figure 6. Measurements of $\langle uv \rangle$ within the inner layer using micro-PTV.

## Normal Stress

The inner layer measurement of streamwise Reynolds stress within $y^+<35$ from micro-PTV is shown in Figure 7. The magnitude of $\langle u^2 \rangle$ peak over the SHS is similar to the smooth surface while its location is closer to the wall over the SHS ($y^+ \sim 9.8$) relative to the smooth surface ($y^+ \sim 15.2$). Further away from the wall at $y^+ > 20$, $\langle u^2 \rangle$ over the SHS becomes comparable with the smooth wall. This trend is consistent with the DNS over longitudinal micro-grooves by Rastegari & Akhavan (2015) as they observed larger $\langle u^2 \rangle$ close to the wall ($y^+ < 8$) while it overlapped with $\langle u^2 \rangle$ of smooth wall at $8 < y^+ < 100$. They associated larger $\langle u^2 \rangle$ near the wall over SHS ($y^+ < 5$) to larger wall-normal gradient of the streamwise velocity ($\partial \langle U \rangle / \partial y$) due to the slip at the wall. The DNS of Min & Kim (2004) shows that $\langle u^2 \rangle$ over SHS is larger than $\langle u^2 \rangle$ over the smooth surface till $y^+ = 10$, but further away from the wall the smooth case becomes larger than the SHS (at $10<y^+<100$). This reduction of $\langle u^2 \rangle$ away from the wall is also observed by the outer layer measurement of Woolford et al. (2009). They reported 20% reduction in $\langle u^2 \rangle$ over a SHS with organized longitudinal pattern at $y / H = 0.2$ while the reduction extends till $y / H = 0.8$ within the other half-channel. The holographic measurement of Ling et al. (2016) showed for all drag reduction superhydrophobic cases with $0.43 \leq k^+_{rms} \leq 1.71$, the value of $\langle u^2 \rangle$ is higher than the smooth case at $y^+<10$ while it is smiler to the smooth surface further away from the wall in $10 \leq y^+ \leq 100$ range.

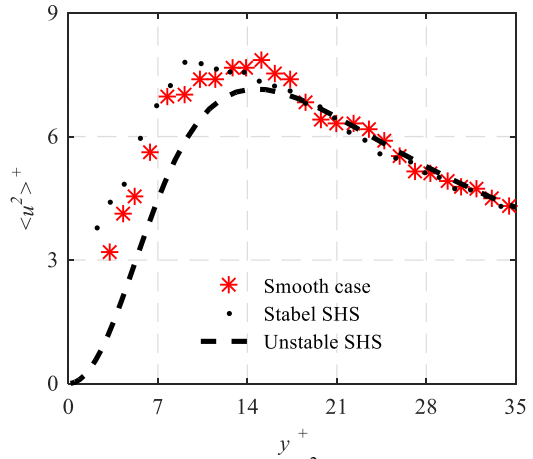


Figure 7. Measurements of $<u^2>$ within the inner layer using micro-PTV.

The normalized $<v^2>$ in the inner layer of $y^+ < 35$ is shown in Figure 8 from micro-PTV. The $<v^2>$ over SHS and smooth surface are observed to overlap near the wall at $y^+<10$. The $<v^2>$ over the SHS becomes smaller than the smooth case beyond $y^+>10$. The reduction of $<v^2>$ peak is in agreement with DNS of Min & Kim (2004) over a superhydrophobic surface when wall slip is numerically imposed in both streamwise and spanwise directions. The experiments of Vajdi Hokmabad & Ghaemi (2016) showed 13% reduction in $<v^2>$ peak over SHS while the peak moved away from the wall by ~15 wall unit. Min & Kim (2004) observed also an overlap of $<v^2>$ over the SHS and smooth surface at $y^+<10$. However, the measurement of Ling et al. (2016) showed in general higher $<v^2>$ over all SHSs with DR at $y^+<30$ followed by a smaller $<v^2>$ at $y^+>30$ compared with the smooth surface.

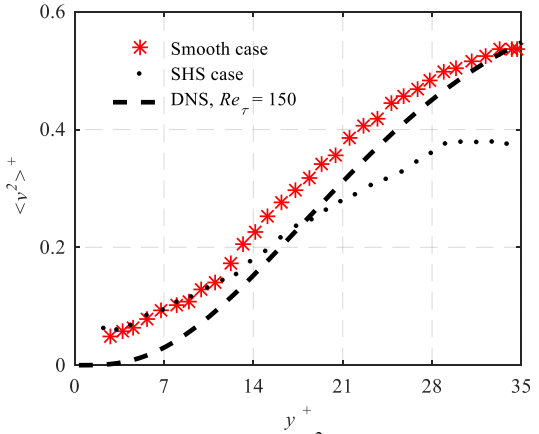


Figure 8. Measurements of $<v^2>$ within the inner layer using micro-PTV.

## Effect of plastron longevity on turbulence

The DR endurance over a SHS depends on the longevity of the air layer (plastron). Several repeats of PIV/PTV experiments showed occasional failure of the surfaces (lack of DR), which is speculated to be due to loss of the air-layer over the SHS. This might have been caused by the presence of PIV/PTV tracers, small variations of pH, and oxygen level of the water (~2000 Liters in the flume). The pH and oxygen level of the water was monitored to be between 7.9-8.1 and 8.3-8.4 mg/L in all the experiments. The manufacturing repeatability, and as a result, the exact roughness of the spray coated SHS may also affect the performance.

Two data sets introduced here as "stable" and "unstable" plastrons are investigated. The stable data belongs to the SHS previously detailed. The unstable data is associated with a SHS that gradually lost its DR performance as it will be evidence by gradual loss of slip-velocity at the wall. The temporal variation of SHS longevity is investigated by averaging velocity ($<U_t^+>$) from micro-PTV within $y^+<15$ and within time intervals of $\Delta t = 100$ sec (moving average). The combination of wall-normal and temporal averaging is applied to enhance statistical convergence of the data. The results are shown in Figure 9 for smooth surface, stable SHS, and unstable SHS. The average velocity $<U_t^+>$ over the smooth surface and stable SHS are relatively constant in time while $<U_t^+>$ of unstable SHS decreases with time over $t = 0$ till 800 sec period. The mean velocities over both SHSs started with larger values ($<U_t^+> = 6.5$, ~0.08 m/s) than the smooth surface ($<U_t^+> = 5.3$, ~0.06 m/s). However, after 400 seconds the unstable SHS stared to lose the plastron as the mean velocity reduces from the range of the stable SHS (~0.08 m/s) to the same mean velocity over the smooth surface (~0.06 m/s). This investigation highlights the need for evaluation of plastron state in large-scale experiments. It also strengthens the need for simultaneous PIV and micro-PTV to ensure measurement is carried out over the same plastron state.

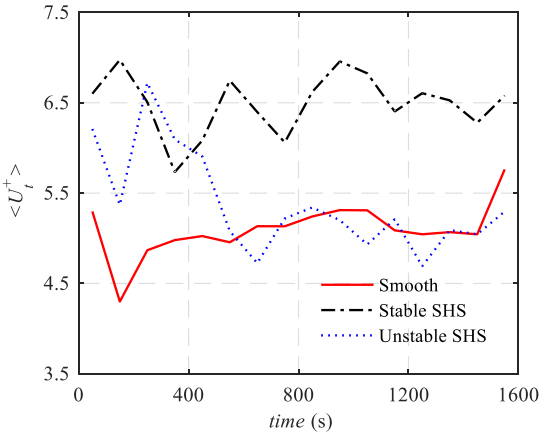


Figure 9. Velocity obtained from micro-PTV averaged within wall-normal range of $y^+$=1-15 with temporal kernel of 100 seconds (500 images pairs) for smooth, stable SHS, and unstable SHS.

## Estimation of skin-friction

The skin-friction reduction (SFR) is estimated using an analytical expression provided by Rastegari & Akhavan (2015) for a surface with slip velocity. They suggested the SFR is the summation of two terms including the slip velocity at the wall and a weighted wall-normal integral of

Reynolds shear stress on SHS relative to the smooth wall. This equation is expressed as

$$\mathrm{SFR} = \frac{U_s}{U_b} + \left(1 - \frac{U_s}{U_b}\right)\left(\frac{3\varepsilon}{1 - 3I^+}\right) \qquad (1)$$

where $\varepsilon = I^{+0} - I^+$ is the difference between the integrals of weighted Reynolds shear stress over the smooth surface and SHS, respectively. $I^+$ is defined as

$$I^+ = \int_0^1 (1 - \delta)\langle uv\rangle^+ d\delta. \qquad (2)$$

Here $\delta = 2y / H$ is the normalized wall-normal coordinate. The integrals are carried out from the first micro-PTV data point to the center of the channel from PIV. Therefore, the integrals are obtained from both measurement techniques within $\delta = 0.01$ to 0.16 (or from $1.4^+$ to $22.5^+$) using micro-PTV and from $\delta = 0.16$ to 1.0 ($22.5^+$ to $140^+$) from PIV. The obtained SFR from equation (1) is 21.9% over the current SHS.

## CONCLUSION

The magnitude of the slip velocity and the effect of the SHS on the turbulence intensities in the inner and outer layers have been experimentally investigated using simultaneous long-range micro-PTV and macroscopic PIV. The micro-PTV results show a slip velocity of 0.023 m/s (13% of $U_b$) over the SHS at $Re_\tau = 140$ which corresponds to 200 μm slip-length. The peak of $\langle u^2\rangle$ over the SHS moved toward the wall relative to the peak over the no-slip surface. The effect of the SHS on the wall-normal Reynolds stress was more pronounced as the SHS significantly reduced $\langle v^2\rangle$ at $y^+ > 10$. The Reynolds shear stress over the SHS is also attenuated compare with the no-slip surface at $y^+ > 10$. The lifetime of the plastron of the SHS is observed to be affected by the turbulent flow since the near-wall velocity over the SHS is reduced with time.

## ACKNOWLEDGMENTS

This work has been supported by the Natural Sciences and Engineering Research Council of Canada (NSERC RGPIN 1512 GHAEMI).

## REFERENCES

Bidkar, R.A., Leblanc, L., Kulkarni, A.J., Bahadur, V., Ceccio, S.L. and Perlin, M., 2014. Skin-friction drag reduction in the turbulent regime using random-textured hydrophobic surfaces. *Physics of Fluids*, *26*(8), p.085108.

Daniello, R.J., Waterhouse, N.E. and Rothstein, J.P., 2009. Drag reduction in turbulent flows over superhydrophobic surfaces. *Physics of Fluids*, *21*(8), p.085103.

Vajdi Hokmabad, B. and Ghaemi, S., 2016. Turbulent flow over wetted and non-wetted superhydrophobic counterparts with random structure. *Physics of Fluids*, *28*(1), p.015112.

Kähler, C.J., Scharnowski, S. and Cierpka, C., 2012. On the uncertainty of digital PIV and PTV near walls. *Experiments in fluids*, *52*(6), pp.1641-1656.

Ling, H., Srinivasan, S., Golovin, K., McKinley, G.H., Tuteja, A. and Katz, J., 2016. High-resolution velocity measurement in the inner part of turbulent boundary layers over super-hydrophobic surfaces. *Journal of Fluid Mechanics*, *801*, pp.670-703.

Meinhart, C.D., Wereley, S.T. and Santiago, J.G., 2000. A PIV Algorithm for Estimating Time-Averaged Velocity Fields. *Journal of Fluids Engineering*, 122(2), p.285.

Min, T. and Kim, J., 2004. Effects of hydrophobic surface on skin-friction drag. *Physics of Fluids*, *16*(7), pp. L55-L58.

Ou, J., Perot, B. and Rothstein, J.P., 2004. Laminar drag reduction in microchannels using ultrahydrophobic surfaces. *Physics of fluids*, *16*(12), pp.4635-4643.

Papadopoulos, P., Mammen, L., Deng, X., Vollmer, D. and Butt, H.J., 2013. How superhydrophobicity breaks down. *Proceedings of the National Academy of Sciences*, *110*(9), pp.3254-3258.

Park, H. and Sun, G., 2014. Superhydrophobic turbulent drag reduction as a function of surface grating parameters. *Journal of Fluid Mechanics*, *747*, pp.722-734.

Rastegari, A. and Akhavan, R., 2015. On the mechanism of turbulent drag reduction with super-hydrophobic surfaces. *Journal of Fluid Mechanics*, *773*, p. R4.

Rothstein, J.P., 2010. Slip on superhydrophobic surfaces. *Annual Review of Fluid Mechanics*, *42*, pp.89-109.

Theunissen, R., Scarano, F. and Riethmuller, M.L., 2008. On improvement of PIV image interrogation near stationary interfaces. *Experiments in Fluids*, *45*(4), pp.557-572.

Tsukahara, T., Seki, Y., Kawamura, H. and Tochio, D., 2005. DNS of turbulent channel flow at very low Reynolds numbers. In *TSFP DIGITAL LIBRARY ONLINE*. Begel House Inc.

Woolford, B., Prince, J., Maynes, D. and Webb, B.W., 2009. Particle image velocimetry characterization of turbulent channel flow with rib patterned superhydrophobic walls. *Physics of Fluids*, *21*(8), p.085106.

Zhang, J., Tian, H., Yao, Z., Hao, P. and Jiang, N., 2015. Mechanisms of drag reduction of superhydrophobic surfaces in a turbulent boundary layer flow. *Experiments in Fluids*, *56*(9), p.179.